Journal of *Marine Science and Engineering*

MDPI

Article

A State-Dependent Hypoplastic Bounding Surface Model for Gassy Sand

Mingyuan Wang [1], Jizhu Sun [2,*] and Yong Wang [3]

[1] Power China Huadong Engineering Corporation Limited, Hangzhou 310014, China
[2] School of Civil Engineering and Architecture, Wuhan University of Technology, Wuhan 430070, China
[3] Institute of Rock and Soil Mechanics, Chinese Academy of Sciences, Wuhan 430071, China
* Correspondence: sunjizhu1@163.com

Abstract: As a kind of partially saturated soil often containing dissolved gas with a high degree of saturation (S > 85%), gassy sand sediment widely exists in the marine environment all over the world. Due to the effect of gas dissolution and exsolution on the pore fluid compressibility, its stress–strain and pore pressure responses are quite different from those of common saturated and unsaturated soils when subjected to undrained loading. Since almost all the gas bubbles are occluded in the pore water of offshore gassy sand, the matric suction may be neglected, and an undrained constitutive model for gassy sand is developed based on the existing hypoplastic bounding surface model for saturated sand. Both Boyle's and Henry's laws are employed in the model to characterize the equilibrium behavior of the gas compressibility and solubility, and then the equivalent compressibility coefficient of the pore fluid is obtained. To avoid unrealistic volumetric expansion, the concepts of the critical state and state-dependent dilatancy stress ratio are incorporated to describe its ultimate shear strength and dilatancy characteristics, respectively. Finally, the triaxial undrained test results on gas-charged sand from Hangzhou Bay are analyzed at three initial saturation degrees of 85%, 90%, and 100%, and two effective confining pressures of 50 kPa and 200 kPa. Moreover, carbon dioxide (CO_2) was selected in the test, and the samples were loose with a relative density of 30%. It is noted that a good agreement is achieved between the simulation results and the experimental data, including the influence of gas content and confining pressure on the shear dilatancy and the mean effective stress increase at the beginning of the effective stress path, among others.

Keywords: marine sediments; gassy sand; partial saturation; state-dependent; bounding surface

Citation: Wang, M.; Sun, J.; Wang, Y. A State-Dependent Hypoplastic Bounding Surface Model for Gassy Sand. *J. Mar. Sci. Eng.* **2023**, *11*, 658. https://doi.org/10.3390/jmse11030658

Academic Editor: Antoni Calafat

Received: 7 February 2023
Revised: 11 March 2023
Accepted: 15 March 2023
Published: 21 March 2023

1. Introduction

As well known, sediments contain free and dissolved gas or gas hydrates, and they have been found in marine environments, including river deltas and shallow and deep seas. The gas-bearing sediments are often called gassy soil and have often been encountered in engineering constructions in the eastern coastal areas of China. The free gas may alter the mechanical properties of the soil significantly, especially the shear strength and volume strain behavior. Under undrained unloading conditions, gas exsolution and expansion may increase the pore fluid pressures while decreasing the effective stresses, which endangers engineering structures [1].

Since the geotechnical effects of the gas in soil were first realized in terrestrial environments [2], the physical and mechanical behaviors of gassy soil have been studied by various researchers [3–6]. However, only a few comprehensive models have been developed for the numerical modeling of geotechnical engineering. The constitutive models of gassy soils are generally classified into two categories: (a) a modified saturated soil model and (b) an unsaturated soil model. Usually, the first category is employed to improve the saturated soil model due to its additional consideration of the gas phase effect, as published by Wheeler (1988) and Pietruszczak et al. (1996) [3,7], where the gassy soil was treated as a three-phase

mixed medium, and the mechanical properties were described in terms of the average stress and strain responses in all constituents. Thereby, the effective stress principle took the same form as saturated soil. Grozic (2005) developed an elastoplastic model for loose gassy sand from Imam et al. (1999) [8,9], and the modifications involved took into account the compressibility and solubility of the pore fluid and gas. The other category considered the existence of matric suction and applied the effective stress principle to unsaturated soil. For example, Wang (2009) proposed a nonlinear elastic model coupling with three phases, such as the solid and liquid of the gassy sand, during gas release [10]. Liu et al. (2011) proposed a hysteretic soil and water characteristic curve model according to the bounding surface plasticity concept [11], which was then incorporated into a constitutive relation that accounted for the coupling effects between the hydro and mechanical behavior of unsaturated sands in the general stress space. Liu et al. (2013) selected the effective stress of the soil skeleton [12], with suction and air pressure as the stress variables and plastic volume strain and saturation degree as the hardening parameters. Subsequently, they developed an elastoplastic model accounting for the effect of gas diffusion with a generalized effective stress principle. Due to the influences of the matric suction, saturation, and other factors, the constitutive model considering the unsaturated soil was more complex than that of the saturated soil.

In fact, many investigations have found that the saturation degree of the gassy marine sediments in deltaic environments is commonly above 85% [13,14], where the free gas in sandy soils exists as occluded bubbles within the pore water. Although these tiny gas bubbles would not markedly interact with the soil aggregates and distort the soil structures, their presence increases the compressibility of the pore fluid significantly, further affecting the undrained pore pressure and strength characteristics of the soil. It is known from Fredlund and Rahardjo (1993) that the pore water pressure coefficient B-value varies largely from 1 to 0.1 in response to the change in the Sr from 100% to 80% [15]. Yoshimichi Tsukamoto (2018) separated the phases of the saturation in soils into three categories of full saturation ($B = 1$), partial saturation ($B < 1$, $S_u \approx 0$), and unsaturation ($B < 1$, $S_u > 0$), in view of the pore pressure coefficient B and the matric suction S_u characteristics [16]. When the soils were unsaturated, the gas phases were continuous within the soil aggregates. In partially saturated soil, the gas phase was discontinuous in the form of discrete bubbles, such that gassy marine soil may be classified as partially saturated soil. Fredlund and Rahardjo (1993) argued that when the degree of water saturation was higher than 85%, the gas bubbles were often occluded in the pore water, the matric suction could be neglected, and the water and gas bubble mixture could be treated as a homogeneous medium [15].

In offshore geotechnical engineering analysis, a soil model is crucial. This study is thus focused on the development of a constitutive model for gassy marine sand with high saturation (S > 85%). Based on the effective stress principle for saturated soil, a hypoplasticity sand model has been proposed to simulate different sand behaviors under monotonic and cyclic loading successfully [17]. Additionally, it is modified to take into account the effects of gas compressibility and dissolution and incorporate the concept of the critical state and state-dependent dilatancy. The triaxial undrained shear properties of the gassy sand and the modified model simulations are compared and discussed in detail.

2. Undrained Behaviors of Gassy Sand

2.1. Compressibility of Pore Fluids

In sandy gassy marine sediments with a high saturation degree, the water is saturated by dissolved gases, and the pore fluid consists of miscible fluids, such as free gas, dissolved gas, and pore water. The two gasses make the pore fluid in gassy sand highly compressible. Fredlund and Rahardjo (1993) reported that if Boyle's rule is applied to the total volume of free and dissolved gas in the three-phase medium, then Henry's rule for dissolved gas can be combined with Boyle's rule for free gas [15]; this concept and the phase diagram are

shown in Figure 1, and the equivalent compressibility coefficient of the miscible fluids C_f can be derived as follows,

$$C_f = \frac{1 - S + Sh}{u} + C_w S \tag{1}$$

where S is the degree of water saturation, h is Henry's volumetric solubility parameter of the gas, u is the current absolute pore water pressure, and C_w is the compressibility coefficient of the pore water. Henry's constant changes with different gas and liquid combinations. For example, for the carbon dioxide–water mixture, h is 0.86, and regarding the methane–water mixture, h is 0.034 [4]. It should be noted that the degree of saturation changes due to the change in the fluid volume in the incremental calculation; the ith step of the saturation is expressed by $S_{i+1} = e_i S_i / [e_i - (1 + e_i)\Delta\varepsilon_v]$ (e_i = void ratio, $\Delta\varepsilon_v$ = volumetric strain).

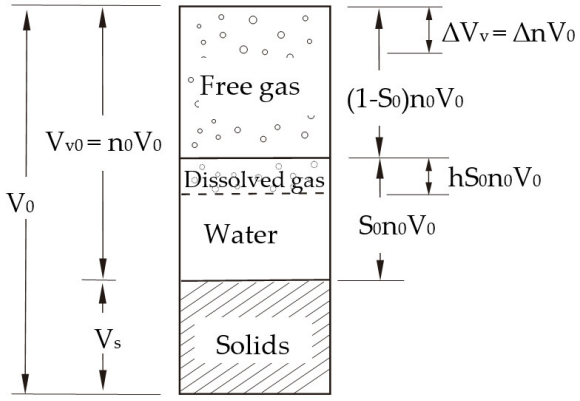

Figure 1. Volumetric composition of the gassy sand.

2.2. Effective and Pore Fluid Stiffness

Under undrained conditions, an increment in pore fluid pressure can cause the compression of the pore fluid and soil particles, and the related effective stress increment generally causes a volume change in the soil particles as well. Effective stress is required to be acted on the particle contact faces. These action areas are very small, and associated volumetric changes are relatively small, such that they can be neglected. Assuming that the solid and fluid phases of the soil deform together when subjected to an undrained condition, the strains are identical in each phase from a macroscopic view, and the total volume change can be given by

$$\Delta\varepsilon_v = C_e \cdot \Delta u = \left[nC_f + (1 - n)C_s \right] \Delta u \tag{2}$$

where C_e is the equivalent volume compressibility coefficient of the pore fluid, C_s is the volume compressibility coefficient of the solid particle, and n is the soil porosity. For saturated soils, both C_s and C_f are much smaller than the soil skeleton compressibility. Their exact value has become unimportant, and it is possible to assume that $C_f = C_s$. For gassy soils, the compressibility of the pore fluid increases dramatically, and because C_f is much greater than C_s, one can assume $C_e = nC_f$.

If neglecting the matric suction effects, the Terzaghi effective stress principle can still be used for the gassy sand, and the expression is given by

$$\{\Delta\sigma\} = \{\Delta\sigma'\} + \{\Delta u\} = \left([D'] + [D_f] \right) \Delta\varepsilon \tag{3}$$

where $[D_f]$ represents a 6×6 stiffness matric of the pore fluid, in which the nine elements in the upper left corner are equal to $1/C_e$, and all the other elements are zero. $[D']$ represents a 6×6 stiffness matric of the soil skeleton, providing a relationship between the effective stress and strain increments. Substituting Equation (1) into (2) and combining it with the Equation (3), seven unknown variables can be solved from the seven algebraic equations, including pore water pressure and six effective stresses or strains.

3. A Constitutive Model for Gassy Sand

3.1. State-Dependent Dilatancy

The test results showed that the dilatancy of the sand depends not only on the shear stress ratio but also on the sample density. Based on the critical state soil mechanics, Been and Jefferies (1985) introduced the state parameter ψ [18], which is a scalar quantity and measures the distance from the current to critical void ratios at the same mean effective stress p. It has been demonstrated experimentally by Verdugo and Ishihara (1996) [19]) that the critical state line for sand was not an approximate straight line in the *e-ln p* plane when the pressure changes within a wide range. In the present study, as shown in Figure 2, ψ is expressed as

$$\psi = e - e_c = e - [e_\Gamma - \lambda(p/p_a)^\xi] \quad (4)$$

where e_Γ, λ, and ξ are the sand parameters defining the critical state line in the *e–p* space (Li & Wang, 1998), and p_a is the atmospheric pressure for nondimensionalization. When $\psi > 0$ (looser than critical), the soils are compressed during drained shearing, or the pore pressures increase during undrained shearing; when $\psi < 0$ (denser than critical), the soils dilate, or the pore pressures decrease.

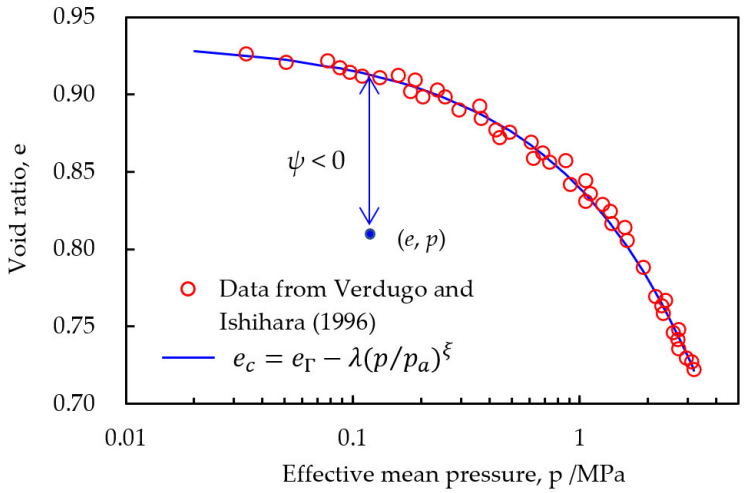

Figure 2. Critical state line and state parameter.

Under undrained loading, the effective stress and pore pressure responses in the soil depend on its shear-induced volumetric dilative and contractive trend. The volumetric of the dense sand changes from contractive to dilative during drained loading (i.e., phase transformation), and the dilatancy line, $R - R_d = 0$, prescribes the place where a contractive phase transforms to a dilative phase only when the stress state lies on the dilatancy line ($R = R_d$), and the soil has no volumetric change. Manzari and Dafalias (1997) argued that a constant R_d results in an unrealistic dilatancy at critical failure, and shear dilatancy should be limited after phase transformation occurs [20]; it is required that R_d is a variable to be consistent with CSSM, and the dilatancy line passe through the critical state point, in other words, shear dilatancy decrease to zero from phase transformation to critical failure state gradually. In this study, a modified state-dependent dilatancy stress ratio R_d is given by

$$R_d = R_f + m\langle e_{c0} - e_0 \rangle \cdot \psi \quad (5)$$

where R_f is the failure stress ratio, R_f and m are two soil constants, e_0 and e_{c0} are the initial and critical void ratios at the same initial mean effective stress, and the Macauley brackets represent the operation $\langle x \rangle = 0$, if $x \leq 0$ and $\langle x \rangle = x$ if $x > 0$. It is seen from Equation (5) that the larger $m\langle e_{c0} - e_0 \rangle$, the farther R_d from R_f; that is, the larger the domain of the dilatancy stress ratio is from phase transformation to failure, makes R_d suitable for soil dilatancy with different initial densities.

3.2. Stress–Strain Relationship

According to Wang et al. (1990), the effective stress rate is decomposed into a deviatoric stress ratio rate and a constant stress ratio rate (a bold-face character denotes the tensor, and a superposed dot denotes the rate)

$$\dot{\boldsymbol{\sigma}} = p\dot{\boldsymbol{r}} + \dot{p}\frac{\boldsymbol{\sigma}}{p} = p\dot{\boldsymbol{r}} + (\boldsymbol{r} + \boldsymbol{I})\dot{p} \tag{6}$$

where $\boldsymbol{\sigma}$ is the effective stress tensor, $p = 1/3(\sigma_1 + \sigma_2 + \sigma_3)$ is the effective mean stress, $\boldsymbol{s} = \boldsymbol{\sigma} - p\boldsymbol{I}$ is the deviatoric stress tensor, and $\boldsymbol{I}$ is the second-order identity tensor. The deviatoric stress ratio tensor is defined as $\boldsymbol{r} = \boldsymbol{s}/p$, and the stress ratio invariant is defined as $R = \sqrt{1/2\,\boldsymbol{r} : \boldsymbol{r}}$, which is used to determine three bounding surfaces: the failure surface, $R - R_f = 0$, the maximum prestress surface, $R - R_m = 0$, and the dilatancy surface, $R - R_d = 0$; in the p-J space ($J = pR$); these surfaces become three lines, as shown in Figure 3a. The model supposes that the bounding surfaces are conical shapes in a three-dimensional principal stress space and circular shapes on the π-plane in the stress ratio space, as shown in Figure 3b; an image stress point $\boldsymbol{r}$ is defined as the intersection of the R_m surface with the straight line connecting the origin point and the current stress state $\boldsymbol{r}$ in virgin loading. The scalar quantities ρ and $\bar{\rho}$ are the distances from point o to $\boldsymbol{r}$ or $\bar{\boldsymbol{r}}$, respectively.

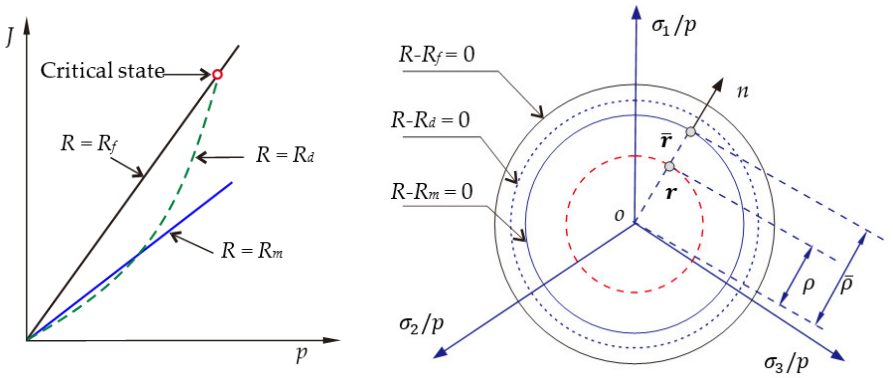

(**a**) Surfaces in *J*-*P* plane (**b**) Surfaces and mapping rule in p = constant plane

Figure 3. Bounding surfaces and mapping rule.

The total strain rate is decomposable into an elastic and a plastic part. Considering Equation (6) and the resolution of the strain into deviatoric and volumetric parts, respectively, the elastic strain rate is defined as

$$\dot{\boldsymbol{\varepsilon}}^e = \frac{1}{2G}p\dot{\boldsymbol{r}} + \left(\frac{1}{2G}\boldsymbol{r} + \frac{1}{3K}\boldsymbol{I}\right)\dot{p} \tag{7}$$

where G and K are the incremental elastic shear and bulk moduli, respectively, and superscript 'e' denotes the elastic component.

Following the framework by Wang et al. (1990), the plastic strain rate is decomposed into two mechanisms related to the stress components, $p\dot{\boldsymbol{r}}$ and $\dot{p}$. Neglecting the second plastic strain associated with $\dot{p}$, the simplified plastic stress–strain relationship is written as

$$\dot{\boldsymbol{\varepsilon}}^p = \left(\frac{1}{H_r}\boldsymbol{n} + \frac{1}{3K_r}\boldsymbol{I}\right)(p\dot{\boldsymbol{r}}:\boldsymbol{n}) \tag{8}$$

where H_r and K_r are the plastic shear and bulk moduli, respectively, related to $\dot{\boldsymbol{r}}$. $\boldsymbol{n}$ is a unit vector along the direction of the deviatoric plastic strain rate in stress space, which is defined as the normal to maximum prestress surface at the image stress ratio $\bar{\boldsymbol{r}}$, and the superscript 'p' denotes the plastic component.

3.3. Elastic and Plastic Moduli

The elastic shear moduli, G, is computed by means of the following empirical expression (Wang, 1990):

$$G = G_0 \frac{(2.973 - e)^2}{1 + e} \sqrt{p p_a} \tag{9}$$

where G_0 is a soil constant, and p_a is the atmospheric pressure. In Equation (9), the current void ratio, e, is introduced instead of the initial void ratio. Based on the elasticity theory, the elastic bulk modulus K can be given by

$$K = G \frac{2(1 + v)}{3(1 - 2v)} \tag{10}$$

where v is Poisson's ratio, and it is assumed to remain constant when pressure and density change in the present model.

In order to obtain the plastic moduli, the elastic moduli is multiplied by some additional terms to describe nonlinear behaviors, such as strain softening. The plastic moduli related to a stress ratio increment takes the following form:

$$H_r = G h_r C \left[\frac{R_f}{R_m} \left(\frac{\overline{\rho}}{\rho} \right)^n - 1 \right] \tag{11}$$

where the strain-dependent term C is modified as

$$C = \frac{1}{1 + \alpha \xi}, \quad \xi = \int \sqrt{\frac{2}{3} de^p : de^p} \tag{12}$$

where C is the scaling factor for the moduli, $n = 2R_m/\overline{\rho}$, h_r and α are dimensionless material constants, and de^p is the deviatoric strain increment.

In order to consider the shear dilatancy and pressure dependency, the elastic bulk modulus K is divided by some term, then the plastic bulk modulus K_r is prescribed by

$$K_r = \frac{K}{w} \tag{13}$$

where w is assumed as the following form:

$$w = \begin{cases} \frac{1}{k_r C} \left(\frac{p}{p_m} \right)^a \left(\frac{R_m}{R_f} \right)^b \left(\frac{R_d - R}{R_f - R_m} \right) \; if \; R = R_m \\ \frac{1}{C} \left(\frac{R_m}{R_f} \right)^d \; otherwise \end{cases} \tag{14}$$

where k_r, a, b, and d are constant parameters, and p_m is the maximum p in the loading history. In the equation, R_d changes with the current void ratio instead of being a constant, as in the original hypoplasticity model.

4. Model Simulations

Since the simulation of cyclic tests was not involved, the modified bounding surface hypoplasticity model in this paper was much simpler than the original one (Wang, 1990), whereas the ability was enhanced to simulate the mechanical behaviors of highly saturated soil. There were a total of 14 soil constants, as listed in Table 1. A systematic calibration procedure for the majority of these parameters was described by Wang (1990) [17] and Li et al. (2000) [21] in detail. The gas dissolution and fluid compressibility coefficient can be taken as constants under normal temperature and pressure, and the two parameters were described in Wang (2009) [1]. The model constants were calibrated by the data from Chen (2021) [22] and are tabulated in Table 1.

Table 1. Model parameters.

Elastic	State	Plastic Shear Modulus	Plastic Bulk Modulus	Liquid–Gas Mixture
$G_0 = 150$ $\nu = 0.3$	$R_f = 0.98$ $m = 8.50$ $e_\Gamma = 1.03, \lambda = 0.02, \xi = 0.7$	$h_r = 0.17$ $\alpha = 1.0$	$K_r = 0.025$ a = 1.0, b = 2.0	$C_w = 4.5 \times 10^{-7}$/kPa $h = 0.86$

Chen (2021) presented a few series of triaxial experiment results on gassy loose sand [22]; the samples were taken from the seabed sandy sediment in Hangzhou Bay, and the main physical properties are listed in Table 2. In the test, carbon dioxide (CO_2) was selected, the effective confining pressures were equal to 50 kPa and 200 kPa, the consolidated undrained triaxial compressions were carried out with a relative density of 30% and three initial degrees of saturation of 85%, 90%, and 100%, respectively, and the axial strain increased at a rate of 0.05 mm/min while maintaining the confining pressure as constants; some of the test results are illustrated in Figures 4–6.

Table 2. Physical properties of gassy sand.

Specific Gravity	Maximum Void Ratio	Minimum Void Ratio	Grain Size (mm)	Relative Density	Fines Content
2.68	1.239	0.739	0.25~0.075	30%	8%

Figures 4 and 5 show the experimental deviatoric stresses, mean effective stresses, pore water pressures, and the simulations given by the modified bounding surface hypoplasticity model with the parameters provided in Table 1. It is seen that the model predictions and the experimental data matched each other quite well for the three saturation degrees or gas contents. For loose sand with D_r = 30%, the existing gas increased the triaxial undrained shear strength, while the peak strength occurred at larger deformation. With the increase in the gas content, the stress–strain behaviors gradually changed from strain softening to hardening, which was probably due to the compression and dissolution of gas, reducing the fluid stiffness significantly. It is noted that it may result in the excess pore pressure accumulation being decreased and delayed and the effective stress being increased, such that the undrained strength was higher than the saturated state. Under undrained conditions, the shear shrinkage or dilatancy could be seen from the changes in excess pore water pressure, as illustrated in Figures 4c and 5b, which increased at the initial loading stage, but slowly in gassy soil because of gas compression or dissolution, later whether it reduced or not depended on the initial saturation degree when the gas content was higher, the excess pore pressure may decrease significantly, this was because the gas exsolution and fluid compressibility increased. Comparing Figures 4 and 5 revealed that when the gas content was identical, the deviatoric stress strength of the gassy soil increased with the higher effective confining pressure. However, strain hardening and shear dilatancy decreased considerably and even disappeared because the particle movement and gas exsolution were strongly constrained in microscopic view (see Figure 5).

The modified model adopted a state-dependent dilatancy stress ratio and a failure stress ratio, which could predict the phase transformation and the failure behavior of gassy sand with different saturation degrees, as illustrated in Figure 4b; because the variable compressibility of the miscible fluid was used to describe the volume change characteristics of the gas–liquid mixture, it could better simulate the increase in the mean effective stress at the beginning of the stress path, when the saturation degree was lower and the later dilatancy characteristics after it crossed the phase transformation line; however, no phase transformation was found, and the strength was lower in the saturated loose sand.

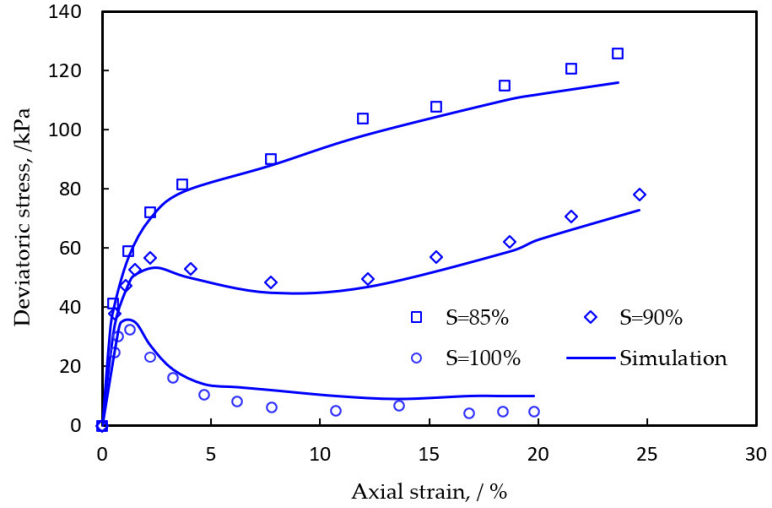

(**a**) Deviatoric stress and axial strain

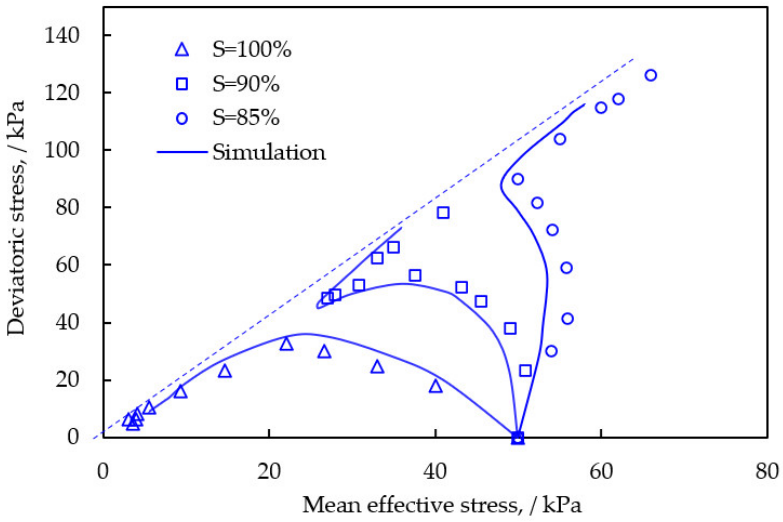

(**b**) Effective stress path

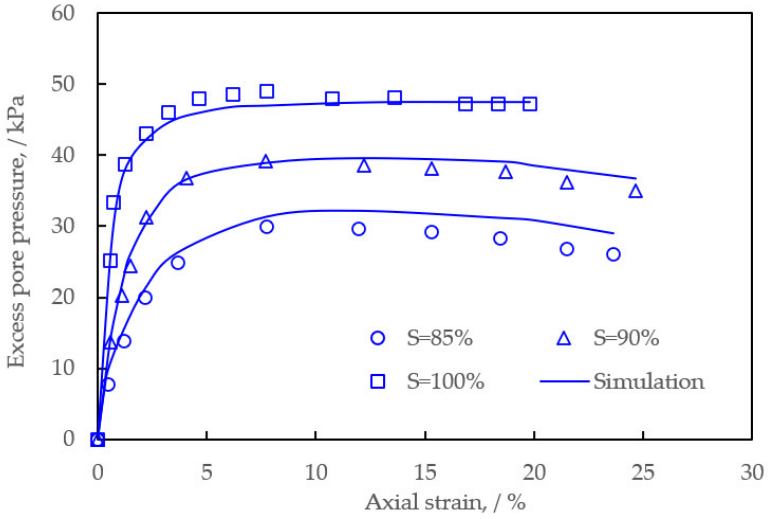

(**c**) Excess pore pressure and axial strain

Figure 4. Undrained triaxial compression test results and model simulations for gassy sand (e_0 = 1.09, p_c = 50 kPa).

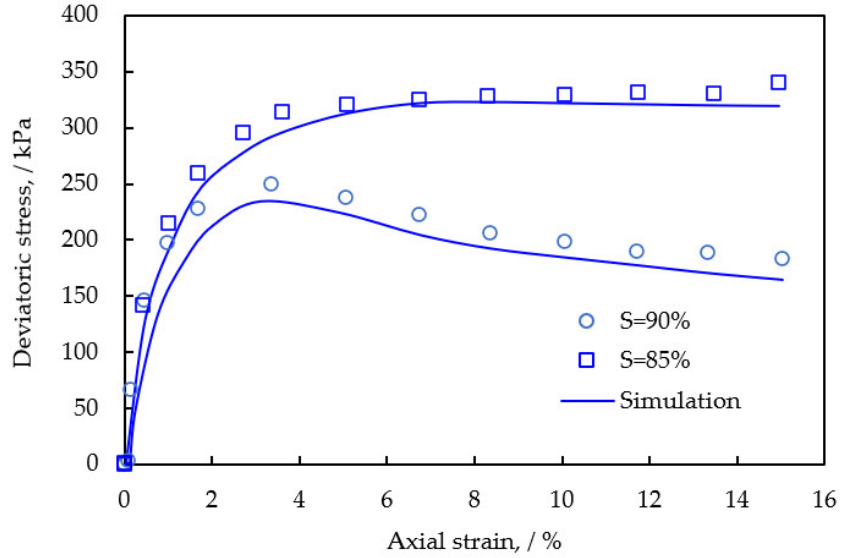

(**a**) Deviatoric stress and axial strain

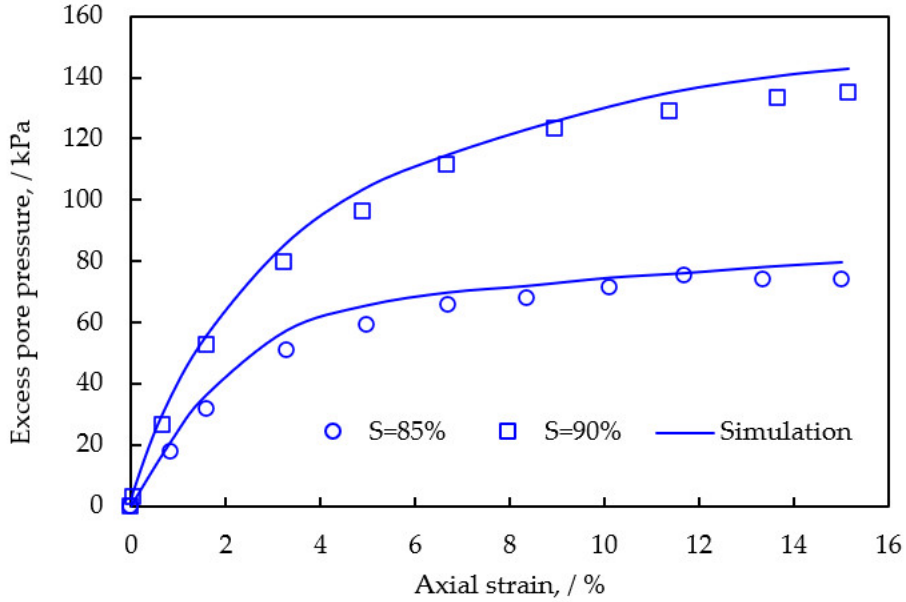

(**b**) Excess pore pressure and axial strain

Figure 5. Undrained triaxial compression test results and model simulations for gassy sand (e_0 = 1.09, p_c = 200 kPa).

It is worth noting that the simulation method proposed by Grozic (2005) is unable to predict the increase in the effective mean normal stress measured at the initial stages of all the triaxial undrained loading; this was because the loading response was still calculated with the pore pressure and volumetric strain relationship of saturated soil, and only the volumetric strain was further corrected according to the calculated pore pressure change, which led to an incorrect pore pressure response at each step of the calculation and incompatible stress and strain results. For saturated soil, the compressibility of the fluid could be theoretically ignored, and the total volume strain change was assumed to be $\dot{\varepsilon}_v = \dot{\varepsilon}_v^e + \dot{\varepsilon}_v^p \approx 0$. When the mean effective stress p' increased, $\dot{\varepsilon}_v^e > 0$; at the same time, when $\dot{\varepsilon}_v^p < 0$ and soil dilatancy occurred, this was contradictory to the initial contraction in the testing. In other words, the pore pressure and strain relation for saturated soil was not applicable to gassy soil. In the present modified bounding surface model, we adopted the compressibility coefficient of the liquid–gas mixture to calculate the pore pressure of gassy sand, which improved the simulation effect of the stress path under the above conditions.

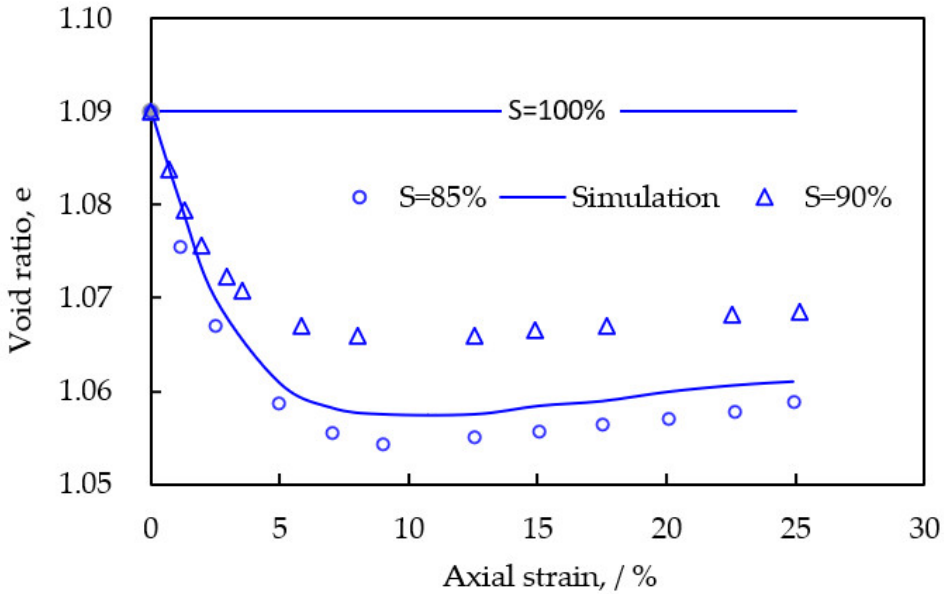

Figure 6. Undrained test results on the void ratio and the axial strain of the gassy sand (e_0 = 1.09, p_c = 50 kPa).

In addition, the higher the gas content of the gassy sand was, the faster the void ratio decreased, or the compactness increased under the undrained condition; the more significant the later dilatancy was, which was similar to the behavior of saturated dense sand, this indicated that the gassy sand changed from shear contraction to dilatancy due to the increase in free gas content. The relation between void ratio change and axial strain is shown at lower confining pressure in Figure 6, where the simulation referred to the saturation degree of 85%. It demonstrates that the modified model can predict that the gassy sand dilates after a small compression as the axial strain increases.

5. Conclusions

A modeling framework was presented in this study for the mechanical properties of gassy sand with a wide range of densities and saturation degrees. In order to describe the influence of closed bubbles on the undrained properties of gassy sand, Boyle's law and Henry's law were combined to obtain the compressibility of the gas–liquid mixed fluid, and the relationship was established between the pore pressure and volumetric strain increment. The modified bounding surface hypoplasticity model was proposed to simulate the behavior of gassy sand. In addition, the concepts of critical state and state-dependent dilatancy were incorporated into the original model by Wang et al. (1990), which made the modified model capable of predicting the dilatancy and failure characteristics at higher strain levels.

The modified model was examined to simulate the undrained triaxial compression on gassy sand. In general, when the saturation degree dropped, the model predictions were in good agreement with the test results, including the undrained strength increase, strain hardening, and volume dilatancy characteristics. In addition, the calculated gas dissolution and exsolution showed reasonable development during undrained loading; especially because the compressibility of the gas–liquid mixed fluid was considered, the model described the increasing characteristics of the mean effective stress at the beginning of the undrained effective stress path. Further work will be conducted to focus on simulating the behavior of gassy sand under cyclic loading and the calculation method of the gas exsolution and pore pressure under the unloading stress path, which is applicable to the simulation of undrained behaviors of gassy sand under complex marine loading.

Author Contributions: Conceptualization, resources, and supervision, M.W.; writing—original draft preparation and project administration, J.S.; writing—review and editing, Y.W. All authors have read and agreed to the published version of the manuscript.

Funding: This research was funded by the National Natural Science Foundation of China, grant number 51979269, 52127815.

Institutional Review Board Statement: Not applicable.

Informed Consent Statement: Not applicable.

Data Availability Statement: All data, models, or code generated or used during the study are available from the corresponding author by request, including all raw data from the tests.

Conflicts of Interest: The authors declare no conflict of interest.

References

1. Wang, Y.; Kong, L.W.; Wang, Y.L.; Wang, M.Y.; Wang, M. Liquefaction response of marine loose gassy sand sediments under cyclic loading. *Bull. Eng. Geol. Environ.* **2018**, *77*, 963–967. [CrossRef]
2. Hardy, R.M.; Hemstock, R.A. *Shearing Strength Characteristics of Athabasca Oil Sands, K.A. Clark Volume*; Information Series 45; Research Council of Alberta: Edmonton, AB, Canada, 1963; pp. 109–112.
3. Wheeler, S.J. A Conceptual Model for Soils Containing Large Gas Bubbles. *Géotechnique* **1988**, *38*, 389–397. [CrossRef]
4. Rad, N.S.; Vianna, A.J.D.; Berre, T. Gas in soils. II: Effect of Gas on Undrained Static and Cyclic Strength of Sand. *J. Geotech. Eng.* **1994**, *120*, 716–737. [CrossRef]
5. Grozic, J.L.; Robertson, P.K.; Morgenstern, N.R. The Behaviour of Loose Gassy Sand. *Can. Geotech. J.* **1999**, *36*, 482–492. [CrossRef]
6. Kong, L.W.; Zhong, F.J.; Guo, A.G. Experimental Study of Stress Path of Shallow Gassy Sand of Hangzhou Bay. *Rock Soil Mech.* **2009**, *30*, 2209–2214.
7. Pietruszczak, S.; Pande, G.N. Constitutive Relations for Partially Saturated Soils Containing Gas Inclusions. *J. Geotech. Eng.* **1996**, *122*, 50–59. [CrossRef]
8. Grozic, J.L.; Imam, S.M.R.; Robertson, P.K.; Morgenstern, N.R. Constitutive Modeling of Gassy Sand Behaviour. *Can. Geotech. J.* **2005**, *42*, 812–829. [CrossRef]
9. Imam, S.M.R. Modeling the Constitutive Behavior of Sand for the Analysis of Static Liquefaction. Ph.D. Thesis, University of Alberta, Edmonton, AB, Canada, 1999.
10. Wang, Y.; Kong, L.W.; Wang, Y.L.; Wang, M.; Cai, K.J. Deformation analysis of shallow gas-bearing ground from controlled gas release in Hangzhou Bay of China. *Int. J. Geomech.* **2018**, *18*, 04017122. [CrossRef]
11. Liu, C.Y.; Muraleetharan, K.K. Coupled Hydro-Mechanical Elastoplastic Constitutive Model for Unsaturated Sands and Silts. I: Formulation. *Int. J. Geomech.* **2012**, *12*, 239–247. [CrossRef]
12. Liu, Y.; Wei, C.F.; Zhao, C.G.; Fang, Q. A Constitutive Model of Unsaturated Soils with High Saturation. *Rock Soil Mech.* **2013**, *34*, 2189–2194.
13. Christian, H.A.; Woeller, D.J.; Robertson, P.K.; Courtney, R.C. Site Investigations to Evaluate Flow Liquefaction Slides at Sand Heads, Fraser River Delta. *Can. Geotech. J.* **1997**, *34*, 384–397. [CrossRef]
14. Fleischer, P.; Orsi, T.; Richardson, M.; Anderson, A. Distribution of free gas in marine sediments: A global overview. *Geo-Mar. Lett.* **2001**, *21*, 103–122.
15. Fredlund, D.G.; Rahardjo, H. *Soil Mechanics for Unsaturated Soils*; John Wiley & Sons, Inc.: New York, NY, USA, 1993; pp. 178–181.
16. Yoshimichi, T. Degree of Saturation Affecting Liquefaction Resistance and Undrained Shear Strength of Silty Sands. *Soil Dyn. Earthq. Eng.* **2019**, *124*, 365–373.
17. Wang, Z.L.; Dafalias, Y.F.; Shen, C.K. Bounding Surface Hypoplasticity Model for Sand. *J. Eng. Mech.* **1990**, *116*, 983–1001. [CrossRef]
18. Been, K.; Jefferies, M.G. A State Parameter for Sands. *Géotechnique* **1985**, *35*, 99–112. [CrossRef]
19. Verdugo, R.; Ishihara, K. The Steady State of Sandy Soils. *Soils Found.* **1996**, *36*, 81–91. [CrossRef] [PubMed]
20. Manzari, M.T.; Dafalias, Y.F. A Critical State Two-Surface Plasticity Model for Sands. *Géotechnique* **1997**, *47*, 255–272. [CrossRef]
21. Li, X.S.; Dafalias, Y.F. Dilatancy for Cohesionless Soils. *Géotechnique* **2000**, *50*, 449–460. [CrossRef]
22. Chen, K.W. Experimental Study on Mechanical Response of Gassy Sand under Different Shearing Paths. Master's Thesis, Guilin University of Technology, Guilin, China, 2021.